[MoO₄]²⁻-templated D_{4h}-symmetric sandwich Ag₁₃ nanocluster coprotected with thiolate and phosphine

Jin-Ping Gao[1], Zhikai Qi[1], Fu-Qiang Zhang[1], and Xian-Ming Zhang [1,2] ✉

[1] *Key Laboratory of Magnetic Molecules & Magnetic Information Materials (Ministry of Education), School of Chemistry & Material Science, Shanxi Normal University, Taiyuan 030032, China*
[2] *College of Chemistry, Taiyuan University of Technology, Taiyuan 030024, China*

ABSTRACT: Mixed-ligand and anion-templated strategies in constructing metal nanoclusters are intricate and ingenious processes that face challenges to be studied. Herein, we report a cationic [Ag₁₃(MoO₄)₄(SC₆H₄iPr)₂(dppp)₈]³⁺ (Ag₁₃) nanocluster, which is templated using four [MoO₄]²⁻ anions and coprotected by 4-isopropylphenol (iPrC₆H₄S⁻) and 1,3-bis (diphenylphosphino) propane (dppp). Two capped (Ag₄SC₆H₄iPr)₂ units connect with the middle Ag@Ag₄ layer via four [MoO₄]²⁻ anion templates to form a three-layer D_{4h}-symmetric structure. An ideal crystallographic fourfold axis passes through the central Ag atom and the S and C atoms of the iPrC₆H₄S⁻ ligand. The layer stacking generates a nonface-centered cubic (nonFCC) structure. The structure and composition of the Ag₁₃ nanocluster have been fully characterized. In addition, the solid ultraviolet–visible (UV–vis) spectra show that Ag₁₃ is a potential narrow-band-gap semiconductor. The photoluminescence (PL) of orange-yellow-light emission is attributed to ligand-to-metal charge transfer. This work has advanced the research on shell engineering of anionic templates and coprotection to assemble high-symmetric Ag nanoclusters.
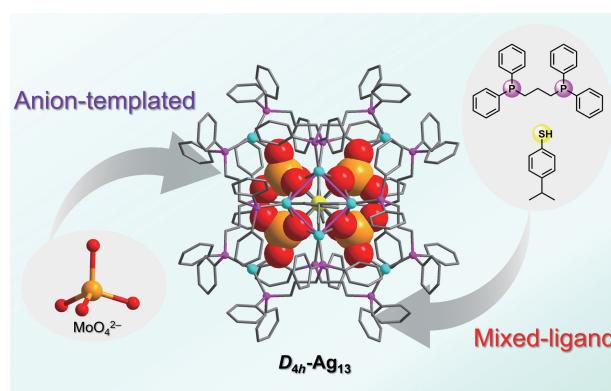
KEYWORDS: anion-templated, [MoO₄]²⁻, coprotected, Ag(I) nanocluster

Anion-templated / MoO₄²⁻ / Mixed-ligand / D_{4h}-**Ag₁₃**

1 Introduction

As truly monodisperse nanomaterials at the molecule level, ligand-protected metal nanoclusters have received extensive attention owing to their structural symmetry, aesthetics, and complexity, which have potential applications in photoluminescence (PL), catalysis, and electrochemistry [1–5]. Choosing the protecting ligands for nanoclusters-between nanoparticles and nanomaterials-is crucial for atom-precise stability. Tailoring the stability, atom packing, and properties of metal clusters by varying the surface organic ligand types explains the effect of different surface organic ligand types on the size, structure, and physicochemical properties of nanoclusters [6–8]. Alkynes, thiols, and phosphines as soft bases are generally easy to coordinate with the soft acid of metal silver. These protected ligands with different coordination abilities and preferences are coordinated to metal atoms, leading to the ever-changing generation of the silver clusters under a single-protection ligand, further reducing the controllability of targeted synthesis [9]. To address this complex problem, new synthesis techniques have been developed that involve adding additional ligands to the cluster synthesis process. By doing so, the stability of the clusters is improved, and unique structural configurations can be achieved. This helps to deepen our understanding of the relationship between structure and properties. Previous reports have proved that the mixed-ligand strategy is an effective method to obtain new functional metal nanoclusters, such as binary ligand-protected Ag₁₄(SC₆H₄X)₁₂(PPh₃)₈ [10], and ternary [Ag₇₈(iPrPhS)₃₀(dppm)₁₀Cl₁₀]⁴⁺ nanoclusters [11]. However, research on the structure of silver clusters generated using mixed protection ligands is still unclear in most cases because of the scarcity of configuration.

Unlike single-ligand protection, Mixed-ligand can use the specificity of the two ligands to control the ratio of the ligands to enrich the structures and properties of the clusters [12, 13]. For thiol/phosphine mixed ligands, adding thiol can overcome the single coordination of phosphine to silver as an auxiliary ligand and increase the abundance of coordination with silver [14–17]. Introducing competing ligands into the thiol salt can also modify

the interfacial silver atom arrangement [18]. Recent studies have demonstrated that the mixed-ligand strategy considerably modifies the number, symmetry, and configuration of silver clusters [19–21]. Various species of diphosphine can achieve the nuclearity of nanoclusters at 18, 24, to 46 for the same kind of thiolate [22]. Thiol and phosphine ligands guide the synthesis of silver clusters with distorted triangular prism structures with C_3 symmetry, such as a series of Ag_9 syntheses [23]. Interestingly, the support of phosphine on the outside forms a large "cage", generating a host–guest interaction model with the inner core, such as Ag@Cu$_{12}$ [24]. In addition, anion-templated strategies have been widely applied in the construction of sliver clusters since it was proposed by Wang in 2015, especially polyoxometalate (POM) anions were encapsulated in sliver clusters to extend the structures and explore the properties [25–29]. The tetrahedral configuration of anions (SO_4^{2-}, SeO_4^{2-}, CrO_4^{2-}, and MoO_4^{2-}) plays a superior role in assembling high-nuclearity and high-symmetry silver nanoclusters [30–32]. The Sun's group successfully synthesized a series of pseudo-seven-fold symmetry Ag$_6$@Ag$_{56}$ [18, 33] and anisotropic Ag$_{52}$ and Ag$_{76}$ clusters [34]. Moreover, [MoO$_4$]$^{2-}$ was used in synthesizing a quasi-five-fold symmetry of the Ag$_{55}$Mo$_6$ cluster [35] and other characterized clusters [36–38]. Therefore, the cooperative coordination of mixed ligands and the effect of [MoO$_4$]$^{2-}$ is hopeful for constructing a subclass of charming Ag cluster.

Herein, we isolated a D_{4h} symmetric structure, [Ag$_{13}$(MoO$_4$)$_4$(SC$_6$H$_4$iPr)$_2$(dppp)$_8$]$^{3+}$ (Ag$_{13}$) (iPrC$_6$H$_4$SH = 4-isopropylphenol and dppp = 1,3-bis(diphenylphosphino)propane), in which the top and bottom layers of square-Ag$_4$SC$_6$H$_4$iPr combined with the central Ag@Ag$_4$ square to form a staggered sandwich configuration. The three stacking layers, including four, five, and four Ag atoms in sequence, can be considered a nonface-centered cubic (nonFCC) structure. iPrC$_6$H$_4$S$^-$ ligands are located in the C_4 axis, and four [MoO$_4$]$^{2-}$ anions are in the two C_2 axes perpendicular to the C_4 principal axis. Remarkably, simple tetrahedron [MoO$_4$]$^{2-}$ was introduced *in situ* to the internal of the nanocluster. Moreover, the solid ultraviolet–visible (UV–vis) spectra exhibit that Ag$_{13}$ is a potential narrow-band-gap semiconductor. The cluster shows a good photocurrent response. In addition, the photoluminescence (PL) properties of orange-yellow-light Ag$_{13}$ were studied at room temperature.

2 Experimental

2.1 Materials and methods

The (iPrC$_6$H$_4$SAg)$_n$ precursor was prepared according to the literature [39]. All other chemicals and solvents used in the syntheses were of analytical grade and used without further purification. A single crystal of Ag$_{13}$ was recorded on a Rigaku Oxford Diffraction XtaLAB Synergy-S diffractometer equipped with a HyPix-6000HE Hybrid Photon Counting detector and an Oxford Cryosystems CryostreamPlus 800 open-flow N$_2$ cooling device at 150 K using Cu Kα (λ = 1.54184 Å). At room temperature, UV–vis absorption spectra were recorded on a TU-1950 UV–vis spectrophotometer. The corresponding optical band gap was evaluated as a function of the Kubelka–Munk equation: $\alpha/S = (1 - R)^2/2R$, in which α represents absorption coefficient, S is scattering coefficient, and R is reflection coefficient. Fourier-transform infrared (FTIR) spectra were obtained on an FTIR spectrophotometer (Thermo Nicolet 360). Energy-dispersive X-ray spectroscopy (EDS) mapping was obtained using JSM-7500F. X-ray

photoelectron spectroscopy (XPS) was performed using the Thermo Scientific K-Alpha$^+$ XPS with a monochromatic Al Kα X-ray source (1486.6 eV), operating at 72 W (12 kV and 6 mA). Binding energies were referred to as the C 1s peak of adventitious carbon at 284.8 eV. Electrospray ionization–time of flight–mass spectrometry (ESI–TOF–MS) was performed using an Agilent Infinity II 6224-6230 Series equipped with time of flight (TOF) modules in positive-ion mode. Data were acquired using the following setting: ESI capillary voltage was set at 4000 V (positive mode) and fragmented at 200 V. Ion chromatography determinations were recorded using Thermo Scientific with a model of DIONEX AQUION RFIC. The leaching solution was 30 mmol, and isocratic reversed-phase was used at a flow rate of 1 mL/min and 30 °C for a 25–30 min collection time with an inhibitor current of 75 mA. The photocurrent test was carried out on a CHI660E electrochemistry workstation. 5 mg samples of Ag$_{13}$ and naphthol (5 wt. %, 10 mL) were dispersed in 80 mL ethanol; this system was mixed for 0.5 h under ultrasound. Then the mixed solution was transferred using pipette tips on a cleaned indium tin oxide (ITO) glass. The coated film was obtained after evaporation at room temperature. The prepared ITO glass film was used as the working electrode, a Pt sheet as the counter electrode, and an Ag/AgCl electrode as the reference electrode. An aqueous 0.2 M Na$_2$SO$_4$ was used as the electrolyte medium.
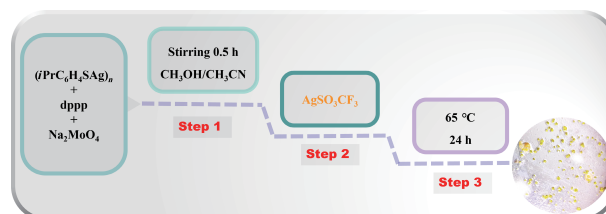
2.2 Synthesis of Ag$_{13}$

A mixture of (iPrC$_6$H$_4$SAg)$_n$ (0.05 mmol, 13 mg), dppp (0.05 mmol, 19 mg), and Na$_2$MoO$_4$ (0.046 mmol, 5 mg) was suspended in 5 mL of CH$_3$CN/MeOH (ratio of 3:2). The solution was stirred for 0.5 h. AgSO$_3$CF$_3$ (0.1 mmol, 27 mg) was added to the solution mixture. The solution was stirred for 24 h continuously. Then, the mixture was sealed in a 25 mL Teflon-lined autoclave under autogenous pressure and heated at 65 °C for 1440 min (Scheme 1). After cooling to room temperature, the yellow block crystals crystallized from the solution after slowly evaporating for a few days, yielding 10% (6.6 mg, based on Ag).

3 Results and discussion

3.1 Crystal structure analysis

The compound Ag$_{13}$ was prepared by reacting iPrC$_6$H$_4$S$^-$, dppp, Na$_2$MoO$_4$, and AgSO$_3$CF$_3$ in a mixed solvent system of acetonitrile and methanol. Yellow block crystal was collected after slowly evaporating the solution for a few days at room temperature. X-ray diffraction (XRD) analysis revealed that Ag$_{13}$ has a molecular formula of [Ag$_{13}$(MoO$_4$)$_4$(SC$_6$H$_4$iPr)$_2$(dppp)$_8$]$^{3+}$ and crystallizes in a monoclinic $P4/nnc$ space groups, exhibiting a square structure with a high-symmetry D_{4h} point group. The atom-precise composition was certificated using ESI–MS. In the positive ion ESI–MS, the strongest peak at a mass/charge (*m/z*) of 1881.12 Da was captured

Scheme 1 Schematic representation of Ag$_{13}$ cluster synthesis.

in the range of m/z = 1500–4500 Da, as shown in Fig. S1 in the Electronic Supplementary Material (ESM). The cluster mass is evaluated to be 5643.36 Da (1881.12 Da × 3), corresponding to the exact composition of $C_{234}H_{230}Ag_{13}Mo_4O_{16}P_{16}S_2$ (theoretical mass = 5643.88 Da), which proves that the cluster is cationic +3 valent, consistent with single-crystal XRD results (Fig. S1 in the ESM). Combining the structural refinement mask information and the results of the ion chromatography measurements determine that the counteracting ion is F⁻ (Fig. S8 in the ESM). The asymmetric Ag_{13} unit contains a quarter of the Ag_{13} cluster, and a crystallographic fourfold axis passes through the central Ag atom (Ag_c) and the S and C atoms of $iPrC_6H_4S^-$. As shown in Fig. 1, the overall structure of this cationic cluster (Ag_{13}) was composed of thirteen Ag atoms coprotected using eight dppp and two $iPrC_6H_4S^-$ ligands as well as bridge-connected anion templates of $[MoO_4]^{2-}$.

The inner core anatomy of Ag_{13} possesses a sandwich square arrangement of $Ag@(MoO_4)_4@(Ag_4SC_6H_4iPr)_2$ (Fig. 2). The Ag_c site adopting η_8 coordination mode is connected with eight μ_2-O atoms from four MoO_4^{2-} anions to build a twisted AgO_8 cubic structure (Figs. 2(a) and 2(b)). The distance of Ag_c–O ranges from 2.28(2)–2.471(8) Å. The four Mo atoms are from anion MoO_4^{2-} units, self-assembled in situ from $Na_2Mo^{VI}O_4$ under a solvothermal process [25]. The Mo–O bond lengths range from 1.520(19) to 1.785(19) Å. Four MoO_4^{2-} anions are arranged in a square at the spacing between the kernel and the shell (Fig. 2(b)). Ag_c links with two $Ag_4SC_6H_4iPr$ units (top and bottom) in the core terminal via eight μ_2-O, generating a double pyramid-like shared-vertex configuration (Fig. 2(c)). Each $Ag_4SC_6H_4iPr$ unit has a compressed tetragonal pyramid geometry, in which the vertex is μ_4-$\eta_1\eta_1$:η_1:η_1 S and all the four Ag–Ag (base) and Ag–S (edge) bond lengths are 3.362 and 2.579 Å, respectively, as well as Ag–S–Ag bond angles are 81.346°. Ag_c atom relates to four terminal silver (Ag_t) atoms via bridging $[MoO_4]^{2-}$ units, forming the middle Ag layer with an Ag_t–O distance of 2.280 Å. Therefore, a sandwich structure with three Ag layers is formed (Figs. 2(d) and 2(e)). In contrast to the classical triple-decker sandwich structural family relying on lanthanide metal or halogen, our three-layer structure is constructed using the template $[MoO_4]^{2-}$ [40, 41]. Such a three-layer structure includes four (top), five (middle), and four (bottom) Ag atoms, different
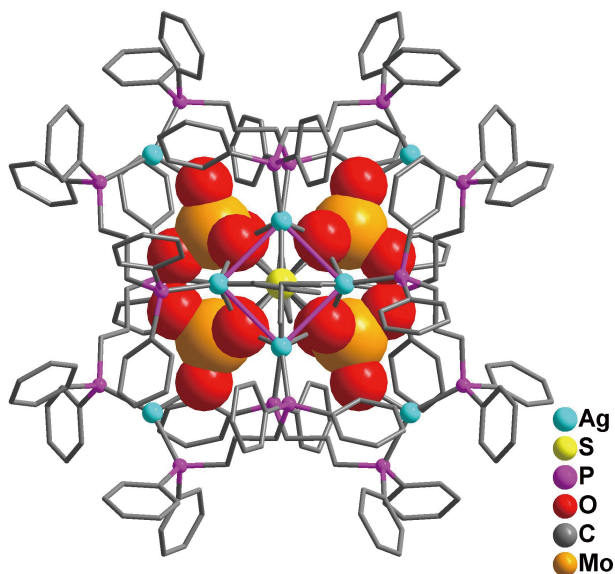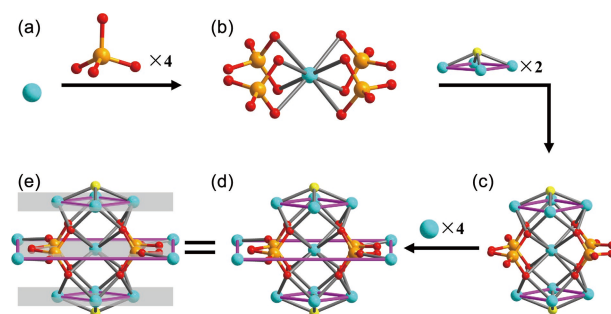

Figure 2 The construction of the Ag_{13} skeleton of the cluster. (a) the center Ag; (b) addition of four MoO_4^{2-} units to Ag_c as the center; (c) two Ag_4S capping around the $Ag_c(MoO_4)_4$ unit; (d) four peripheral Ag_t atoms around $Ag@(MoO_4)_4@(Ag_4SC_6H_4iPr)_2$; (e) sandwich squarate structure of $Ag@(MoO_4)_4@(Ag_4SC_6H_4iPr)_2@Ag_4$. Color codes: blue, Ag; yellow, S; orange, Mo; red, O; C, and H atoms are omitted for clarity.

from the classical FCC structure of three, seven, and three atom stacking, which therefore is defined as a nonFCC structure [42, 43]. Moreover, the spacing between the top/bottom Ag_4 layer and the middle Ag_5 layer is 2.993 Å.

In addition, four Ag_t atoms are linked with an outer shell of eight ditopic dppp ligands (Fig. 3(a)). Two categories of Ag–P bonds were formed between the P atoms of dppp ligands and Ag atoms (Fig. 3(b)). The top/bottom layer Ag–P bond length is 2.337(3) Å, and the middle layer Ag_t–P distance is 2.407(3) Å. In addition, phosphine ligands advance the coordination capacity of Ag and provide various geometry configurations. Each cell consisted of two complete Ag_{13} clusters and six 1/4 dppp ligands. The isolated cluster and cluster stacking pattern along the [001] direction contain a fantastic three-dimensional hole structure (Fig. S2 in the ESM), which is similar to the classical soc topology of the metal–organic framework (MOF) structures [44, 45]. A comparison of size-closed anionic/cationic and neutral silver clusters is summarized with our work in Table S2 in the ESM; thus, the structure of Ag_{13} is not a classical size-closed core–shell but rather a triple sandwich cationic cluster.

The relationship between four $[MoO_4]^{2-}$ anions and three layers of Ag atoms reflects the importance of $[MoO_4]^{2-}$ anions in directing the synthesis of silver nanoclusters. $[MoO_4]^{2-}$ anions are used as a key bridge to connect Ag atoms at the top and bottom as well as four Ag at the middle layer through templating Ag–O interactions. The combination of $iPrC_6H_4S^-$ and dppp plays an initial role in constructing D_{4h} symmetric structure. Two types of Ag–ligand interactions affect the direction of the C_4 and C_2 axes.

3.2 The composition of the Ag_{13} cluster

To study the composition of Ag_{13}, we acquired the EDS element

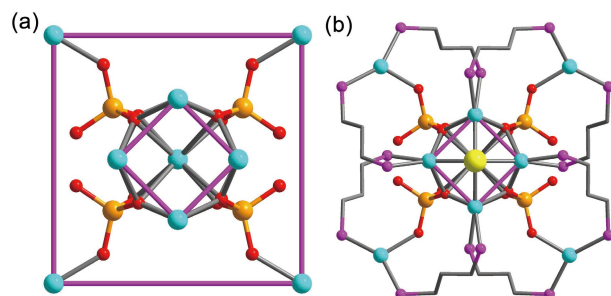**Figure 1** The total structure of Ag_{13}. Hydrogen atoms are omitted for clarity.

Ag
S
P
O
C
Mo

Figure 3 (a) A diagram of $Ag_{13}Mo_4$ unit; (b) $Ag_{13}Mo_4(dppp)_8$ unit consisting of eight dppp ligands connected with Ag and MoO_4 units.

analysis and found that typical Ag, Mo, S, P, C, and O elements are uniformly distributed on the surface of the sample (Fig. S5 in the ESM and Fig. 4(a)). Furthermore, the valences of metal ions were surveyed using XPS. High-resolution spectrum for Ag shows that Ag $3d_{5/2}$ and Ag $3d_{3/2}$ binding energies are 368.23 and 374.25 eV (Fig. 4(b)), respectively, indicating Ag(I) bonding with iPrC$_4$H$_6$S$^-$ [46]. The peaks observed at 232.9 and 235.2 eV for Mo 3d can be ascribed to the binding energies of Mo^{6+} $3d_{5/2}$ and Mo^{6+} $3d_{3/2}$, respectively, which agrees on the combination of Mo–O (Fig. S6(a)

in the ESM) [18]. Figure S6(b) in the ESM shows the XPS data of S-containing bands centered at 162.43 and 168.92 eV for S $2p_{3/2}$ and S $2p_{1/2}$, respectively, assigned to metal sulfides [47]. Furthermore, the disappearance of S–H located at 2678 cm^{-1} and the appearance of the C–P vibrational peak observed at 1438 cm^{-1} in the FTIR spectra prove the incorporation of mixed ligands into the cluster (Fig. S3 in the ESM). Furthermore, the peaks located at the range of 800–900 cm^{-1} for Ag$_{13}$ could be attributed to the Mo=O stretching vibrations of [MoO$_4$]$^{2-}$ anions. The powder XRD pattern of Ag$_{13}$
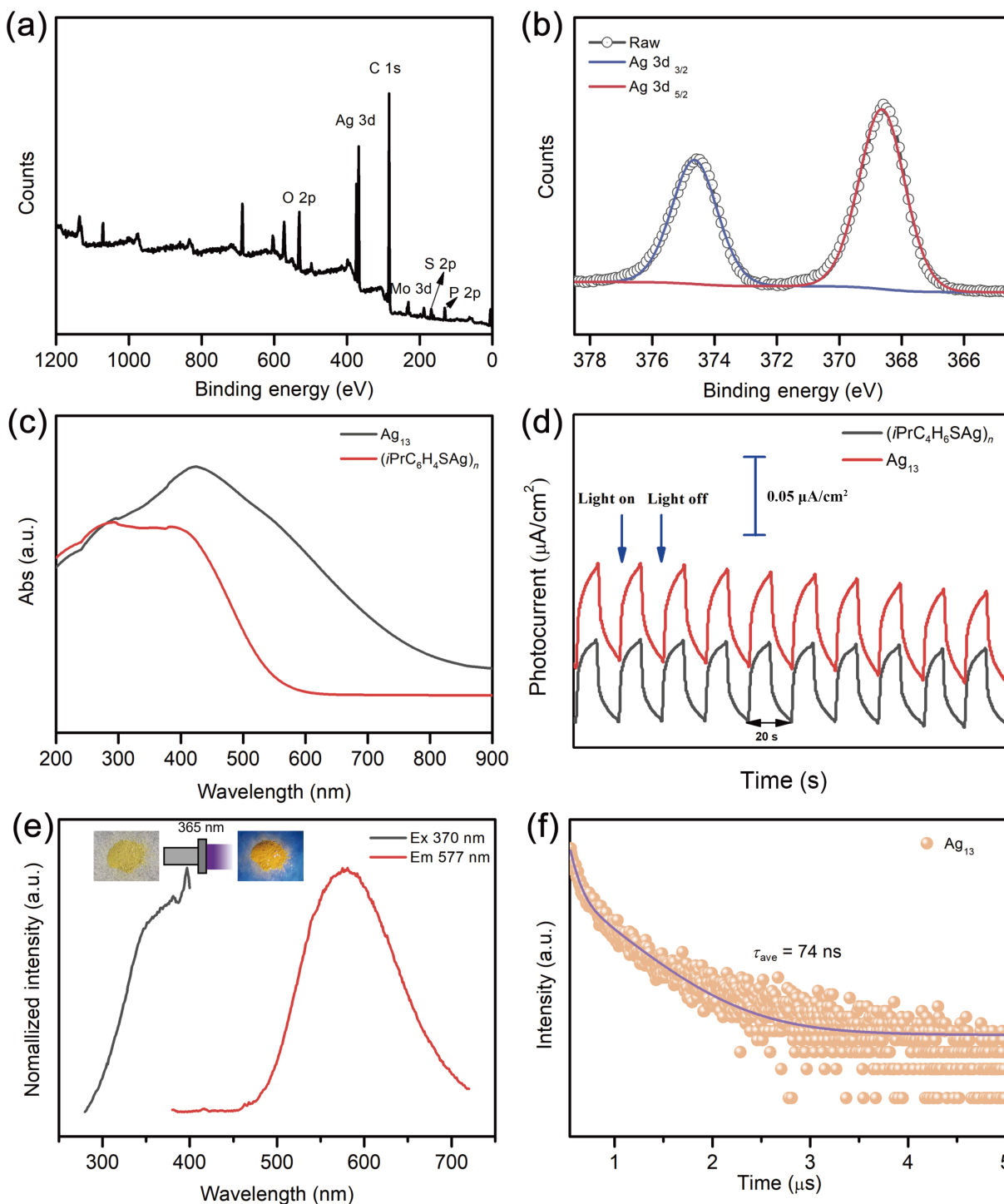

Figure 4 (a) XPS survey spectrum of Ag$_{13}$ and (b) corresponding high-resolution XPS spectrum of Ag 3d. (c) Solid UV–vis absorption spectra and (d) photocurrent responses of (iPrC$_6$H$_4$SAg)$_n$ and Ag$_{13}$. (e) Normalized PL spectrum and (f) the decay lifetime of Ag$_{13}$ under room temperature. The blue line indicates the fitting curve.

matched its simulation pattern (Fig. S4 in the ESM). These results agreed well with the single-crystal structural analysis.

3.3 UV–vis absorption spectra and luminescence properties of Ag₁₃ cluster

To investigate the semiconducting and photophysical properties of the titled cluster, we collected solid-state UV absorption spectra at room temperature and found that Ag₁₃ showed broadband absorption similar to $(i\text{PrC}_6\text{H}_4\text{SAg})_n$ in the wavelength range of 300–500 nm (Fig. 4(c)), which could be determined as the $\pi \rightarrow \pi^*$ transition of $i\text{PrC}_6\text{H}_4\text{S}^-$ ligands [48]. Moreover, using the Tauc equation, the optical bandgaps of Ag₁₃ and precursor $(i\text{PrC}_6\text{H}_4\text{SAg})_n$ were estimated to be 1.44 and 2.10 eV, respectively (Fig. S7 in the ESM), indicating that our synthesized nanocluster is a potentially narrow-band-gap semiconductor. Considering the broad absorption in the UV–vis region, the photoelectrochemical properties of Ag₁₃ were tested in a typical three-electrode system. Compared with the $(i\text{PrC}_6\text{H}_4\text{SAg})_n$-modified ITO electrode, an apparent photocurrent response was detected upon on–off irradiation cycling using 400–800 nm Xe lamp source (50 W) at an interval of 20 s (Fig. 4(d)), indicating a better electron and hole separation efficiency of Ag₁₃. The photocurrent density reached up to 0.07 mA/cm², and the intensity kept nearly constant with increased test times, indicating a high photophysical stability of Ag₁₃.

Besides, Ag₁₃ enables an orange-yellow-light emission under UV light irradiation at 365 nm at room temperature (Fig. 4(e), inset). Therefore, we studied the PL properties of Ag₁₃ in the solid state. Figure 4(e) shows that the emission band peaked at 577 nm under the largest excitation wavelength of 370 nm and with the full width at half maximum of 127 nm. The PL decay curve fitted using a double exponential function enables a lifetime (τ) of 74 ns (Fig. 4(f)) [49, 50]. This emission should be assigned to the ligand-to-metal charge transfer, where the charge is transferred from the S 3p to the Ag 5s orbitals, a characteristic of the polynuclear silver complexes with metallophilic interactions [51, 52]. Furthermore, the electronic structure of the Ag₁₃ cluster was investigated using the density functional theory calculation analysis of the Ag₁₃ cluster. The frontier molecular orbitals highest occupied vacant orbital (HOMO) and lowest vacant orbital (LUMO) diagrams of compound Ag₁₃ are shown in Fig. S9 in the ESM. The HOMO of Ag₁₃ from the molecular orbital analysis is mainly located on the $i\text{PrC}_6\text{H}_4\text{S}^-$ ligand, while the LUMO is mainly located on the central metal atom Ag and C. This result suggests that the Ag₁₃ cluster may achieve charge transfer interactions associated with electron donor and acceptor units, resulting in excellent photoelectric reactivity.

4 Conclusion

We isolated a cationic sandwich silver nanocluster using thiolate and phosphine, $[\text{Ag}_{13}(\text{MoO}_4)_4(\text{SC}_6\text{H}_4i\text{Pr})_2(\text{dppp})_8]^{3+}$, which was templated using multiple $[\text{MoO}_4]^{2-}$ anions. The cluster was constructed using $i\text{PrC}_4\text{H}_6\text{S}^-$ bidentate phosphine dppp, and multiple $[\text{MoO}_4]^{2-}$ anions. Four templated-$\text{MoO}_4{}^{2-}$ anions and eight dppp coordinated with Ag atoms to form a D_{4h}-symmetric sandwich structure. Ag₁₃ was characterized using ESI-MS, FTIR, XPS, and EDS mapping, resulting in the composition matching well with the single-crystal XRD analysis. Solid-state UV–vis shows a potential narrow-band-gap semiconductor and a good photocurrent response. PL spectra revealed that Ag₁₃ emits orange-yellow light at room temperature. This work demonstrates that

simple $[\text{MoO}_4]^{2-}$ anions also can induce novel structures, opening the door to using anions to isolate structures of interesting clusters. We aspire to generate more silver clusters with high-symmetry aesthetics using a strategy of mixed-ligand combinations induced by an anionic template in the future.

Declaration of competing interest

The authors have no competing interests to declare that are relevant to the content of this article.

Author contribution statement

X.-M. Z. and F.-Q. Z. proposed the research project and guided the whole experiments. J.-P. G conducted the syntheses and characterization of complexes, and drafted the manuscript. Z. K. Q. revised the manuscript. All the authors reviewed and contributed to this paper.

References

[1] Jin, Y.; Zhang, C.; Dong, X. Y.; Zang, S. Q.; Mak, T. C. W. Shell engineering to achieve modification and assembly of atomically-precise silver clusters. *Chem. Soc. Rev.* **2021**, *50*, 2297–2319.

[2] Jin, R. C.; Zeng, C. J.; Zhou, M.; Chen, Y. X. Atomically precise colloidal metal nanoclusters and nanoparticles: Fundamentals and opportunities. *Chem. Rev.* **2016**, *116*, 10346–10413.

[3] Jin, J. L.; Xie, Y. P.; Cui, H.; Duan, G. X.; Lu, X.; Mak, T. C. W. Structure-directing role of phosphonate in the synthesis of high-nuclearity silver(I) sulfide-ethynide-thiolate clusters. *Inorg. Chem.* **2017**, *56*, 10412–10417.

[4] Yamazoe, S.; Koyasu, K.; Tsukuda, T. Nonscalable oxidation catalysis of gold clusters. *Acc. Chem. Res.* **2014**, *47*, 816–824.

[5] Jin, R. C. Atomically precise metal nanoclusters: Stable sizes and optical properties. *Nanoscale* **2015**, *7*, 1549–1565.

[6] Guan, Z. J.; Zeng, J. L.; Nan, Z. A.; Wan, X. K.; Lin, Y. M.; Wang, Q. M. Thiacalix[4]arene: New protection for metal nanoclusters. *Sci. Adv.* **2016**, *2*, e1600323.

[7] Jing, X. M.; Fu, F. Y.; Wang, R. J.; Xin, X.; Qin, L.; Lv, H. J.; Yang, G. Y. Robust enantiomeric two-dimensional assembly of atomically precise silver clusters. *ACS Nano* **2022**, *16*, 15188–15196.

[8] Yuan, Z. R.; Wang, Z.; Han, B. L.; Zhang, C. K.; Zhang, S. S.; Zhu, Z. Y.; Yu, J. H.; Li, T. D.; Li, Y. Z.; Tung, C. H. et al. Ag₂₂ nanoclusters with thermally activated delayed fluorescence protected by Ag/cyanurate/phosphine metallamacrocyclic monolayers through *in-situ* ligand transesterification. *Angew. Chem. , Int. Ed.* **2022**, *61*, e202211628.

[9] Zeng, J. L.; Guan, Z. J.; Du, Y.; Nan, Z. A.; Lin, Y. M.; Wang, Q. M. Chloride-promoted formation of a bimetallic nanocluster Au₈₀Ag₃₀ and the total structure determination. *J. Am. Chem. Soc.* **2016**, *138*, 7848–7851.

[10] Das, A. K.; Mekkat, R.; Maity, S.; Nair, A. S.; Bhandary, S.; Bhowal, R.; Patra, A.; Pathak, B.; Chopra, D.; Mandal, S. Role of ligand on photophysical properties of nanoclusters with fcc kernel: A case study

of $Ag_{14}(SC_6H_4X)_{12}(PPh_3)_8$ (X = F, Cl, Br). *Inorg. Chem.* **2021**, *60*, 19270–19277.

[11] Zhang, W. J.; Liu, Z.; Song, K. P.; Aikens, C. M.; Zhang, S. S.; Wang, Z.; Tung, C. H.; Sun, D. A 34-electron superatom Ag_{78} cluster with regioselective ternary ligands shells and its 2D rhombic superlattice assembly. *Angew. Chem. , Int. Ed.* **2021**, *60*, 4231–4237.

[12] Xie, Y. P.; Jin, J. L.; Lu, X.; Mak, T. C. W. High-nuclearity silver thiolate clusters constructed with phosphonates. *Angew. Chem. , Int. Ed.* **2015**, *54*, 15176–15180.

[13] Jin, J. L.; Shen, Y. L.; Xie, Y. P.; Lu, X. Anion templated synthesis of silver(I)-ethynide dithiophosphate clusters. *Cryst. Growth Des.* **2018**, *18*, 4372–4377.

[14] Das, A.; Li, T.; Nobusada, K.; Zeng, Q.; Rosi, N. L.; Jin, R. C. Total structure and optical properties of a phosphine/thiolate-protected Au_{24} nanocluster. *J. Am. Chem. Soc.* **2012**, *134*, 20286–20289.

[15] Shichibu, Y.; Negishi, Y.; Watanabe, T.; Chaki, N. K.; Kawaguchi, H.; Tsukuda, T. Biicosahedral gold clusters $[Au_{25}(PPh_3)_{10}(SC_nH_{2n+1})_5Cl_2]^{2+}$ (n = 2–18): A stepping stone to cluster-assembled materials. *J. Phys. Chem. C* **2007**, *111*, 7845–7847.

[16] Yang, H. Y.; Lei, J.; Wu, B. H.; Wang, Y.; Zhou, M.; Xia, A. D.; Zheng, L. S.; Zheng, N. F. Crystal structure of a luminescent thiolated Ag nanocluster with an octahedral Ag_6^{4+} core. *Chem. Commun.* **2013**, *49*, 300–302.

[17] Bootharaju, M. S.; Dey, R.; Gevers, L. E.; Hedhili, M. N.; Basset, J. M.; Bakr, O. M. A new class of atomically precise, hydride-rich silver nanoclusters Co-protected by phosphines. *J. Am. Chem. Soc.* **2016**, *138*, 13770–13773.

[18] Wang, Z.; Su, H. F.; Kurmoo, M.; Tung, C. H.; Sun, D.; Zheng, L. S. Trapping an octahedral Ag_6 kernel in a seven-fold symmetric Ag_{56} nanowheel. *Nat. Commun.* **2018**, *9*, 2094.

[19] Alhilaly, M. J.; Bootharaju, M. S.; Joshi, C. P.; Besong, T. M.; Emwas, A. H.; Juarez-Mosqueda, R.; Kaappa, S.; Malola, S.; Adil, K.; Shkurenko, A. et al. $[Ag_{67}(SPhMe_2)_{32}(PPh_3)_8]^{3+}$:Synthesis, total structure, and optical properties of a large box-shaped silver nanocluster. J. Am. *Chem. Soc.* **2016**, *138*, 14727–14732.

[20] Bestgen, S. ; Fuhr, O. ; Breitung, B. ; Chakravadhanula, V. S. K. ; Guthausen, G. ; Hennrich, F. ; Yu, W. ; Kappes, M. M. ; Roesky, P. W. ; Fenske, D. $[Ag_{115}S_{34}(SCH_2C_6H_4{}^tBu)_{47}(dpph)_6]$: Synthesis, crystal structure and NMR investigations of a soluble silver chalcogenide nanocluster. *Chem. Sci.* **2017**, *8*, 2235–2240.

[21] Teo, B. K.; Yang, H. Y.; Yan, J. Z.; Zheng, N. F. Supercubes, supersquares, and superrods of face-centered cubes (FCC): Atomic and electronic requirements of $[M_m(SR)_l(PR'_3)_8]^q$ nanoclusters (M = coinage metals) and their implications with respect to nucleation and growth of FCC metals. *Inorg. Chem.* **2017**, *56*, 11470–11479.

[22] Li, X. Y.; Wang, Z.; Su, H. F.; Feng, S.; Kurmoo, M.; Tung, C. H.; Sun, D.; Zheng, L. S. Anion-templated nanosized silver clusters protected by mixed thiolate and diphosphine. *Nanoscale* **2017**, *9*, 3601–3608.

[23] Li, X. Y.; Su, H. F.; Zhou, R. Q.; Feng, S.; Tan, Y. Z.; Wang, X. P.; Jia, J.; Kurmoo, M.; Sun, D.; Zheng, L. S. General assembly of twisted trigonal-prismatic nonanuclear silver(I) clusters. *Chem. —Eur. J.* **2016**, *22*, 3019–3028.

[24] Han, B. L.; Wang, Z.; Gupta, R. K.; Feng, L.; Wang, S. N.; Kurmoo, M.; Gao, Z. Y.; Schein, S.; Tung, C. H.; Sun, D. Precise implantation of an archimedean $Ag@Cu_{12}$ cuboctahedron into a platonic Cu_4Bis(diphenylphosphino)hexane$_6$ tetrahedron. *ACS Nano* **2021**, *15*, 8733–8741.

[25] Wang, Q. M.; Lin, Y. M.; Liu, K. G. Role of anions associated with the formation and properties of silver clusters. *Acc. Chem. Res.* **2015**, *48*, 1570–1579.

[26] Shi, J. Y.; Kumar Gupta, R.; Deng, Y. K.; Sun, D.; Wang, Z. Recent advances in the asymmetrical templation effect of polyoxometalate in silver clusters. *Polyoxometalates* **2022**, *1*, 9140010.

[27] Li, J.; Zhang, D.; Chi, Y. N.; Hu, C. W. Catalytic application of polyoxovanadates in the selective oxidation of organic molecules. *Polyoxometalates* **2022**, *1*, 9140012.

[28] Zhang, S. S.; Chen, J. Y.; Li, K.; Yuan, J. D.; Su, H. F.; Wang, Z.; Kurmoo, M.; Li, Y. Z.; Gao, Z. Y.; Tung, C. H. et al. Janus cluster: Asymmetric coverage of a Ag_{43} cluster on the symmetric preyssler P_5W_{30} polyoxometalate. *Chem. Mater.* **2021**, *33*, 9708–9714.

[29] Zhao, Y. Q.; Yu, K.; Wang, L. W.; Wang, Y.; Wang, X. P.; Sun, D. Anion-induced supramolecular isomerism in two preyssler P_5W_{30} polyoxometalate-based hybrid materials. *Inorg. Chem.* **2014**, *53*, 11046–11050.

[30] Liao, J. H.; Chang, H. W.; You, H. C.; Fang, C. S.; Liu, C. W. Tetrahedral-shaped anions as a template in the synthesis of high-nuclearity silver(I) dithiophosphate clusters. *Inorg. Chem.* **2011**, *50*, 2070–2072.

[31] Chang, H. W.; Liao, J. H.; Li, B.; Chen, Y. J.; Liu, C. W. Trigonal pyramidal oxyanions as structure-directing templates for the synthesis of silver dithiolate clusters. *J. Struct. Chem.* **2014**, *55*, 1426–1432.

[32] Liao, J. H.; Chen, H.; You, H. J.; Liu, C. W. Oxocarbon anions templated in silver clusters. *Inorg. Chem.* **2022**, *61*, 14115–14120.

[33] Wang, Z.; Yang, F. L.; Yang, Y.; Liu, Q. Y.; Sun, D. Hierarchical multi-shell 66-nuclei silver nanoclusters trapping subvalent Ag_6 kernels. *Chem. Commun.* **2019**, *55*, 10296–10299.

[34] Liu, J. W.; Feng, L.; Su, H. F.; Wang, Z.; Zhao, Q. Q.; Wang, X. P.; Tung, C. H.; Sun, D.; Zheng, L. S. Anisotropic assembly of Ag_{52} and Ag_{76} nanoclusters. *J. Am. Chem. Soc.* **2018**, *140*, 1600–1603.

[35] Zhou, K.; Geng, Y.; Yan, L. K.; Wang, X. L.; Liu, X. C.; Shan, G. G.; Shao, K. Z.; Su, Z. M.; Yu, Y. N. An ultrastable {$Ag_{55}Mo_6$} nanocluster with a Ag-centered multishell structure. *Chem. Commun.* **2014**, *50*, 11934–11937.

[36] Gao, G. G.; Cheng, P. S.; Mak, T. C. W. Acid-induced surface functionalization of polyoxometalate by enclosure in a polyhedral silver-alkynyl cage. *J. Am. Chem. Soc.* **2009**, *131*, 18257–18259.

[37] Wang, Z.; Su, H. F.; Wang, X. P.; Zhao, Q. Q.; Tung, C. H.; Sun, D.; Zheng, L. S. Johnson solids: Anion-templated silver thiolate clusters capped by sulfonate. *Chem.—Eur. J.* **2018**, *24*, 1640–1650.

[38] Jin, J. L.; Shen, Y. L.; Xie, Y. P.; Lu, X. Silver ethynide clusters constructed with fluorinated β-diketonate ligands. *CrystEngComm* **2018**, *20*, 2036–2042.

[39] Tang, K. ; Xie, X. ; Zhao, L. ; Zhang, Y. Jin, X. Synthesis and crystal structure of $\{[HNEt_3]_{2n}[Ag_8Ag_4/2(SC_6H_4tBu-4)_{12}]_n \cdot nC_2H_5OH\}$ and its reaction product with CS_2. *Eur. J. Inorg. Chem.* **2004**, *2004*, 78–85.

[40] Kilpatrick, A. F. R.; Green, J. C.; Turner, Z. R.; Buffet, J. C.; O'Hare, D. Zirconium arene triple-decker sandwich complexes: Synthesis, electronic structure and bonding. *Chem. Commun.* **2017**, *53*, 12048–12051.

[41] Guo, L. Y.; Su, H. F.; Kurmoo, M.; Wang, X. P.; Zhao, Q. Q.; Lin, S. C.; Tung, C. H.; Sun, D.; Zheng, L. S. Multifunctional triple-decker inverse 12-metallacrown-4 sandwiching halides. *ACS Appl. Mater. Interfaces* **2017**, *9*, 19980–19987.

[42] Liao, L. W.; Zhuang, S. L.; Wang, P.; Xu, Y. N.; Yan, N.; Dong, H. W.; Wang, C. M.; Zhao, Y.; Xia, N.; Li, J. et al. Quasi-dual-packed-kerneled $Au_{49}(2, 4$-DMBT$)_{27}$ nanoclusters and the influence of kernel packing on the electrochemical gap. *Angew. Chem. , Int. Ed.* **2017**, *56*, 12644–12648.

[43] Qu, M.; Zhang, F. Q.; Wang, D. H.; Li, H.; Hou, J. J.; Zhang, X. M. Observation of non-FCC copper in alkynyl-protected Cu_{53} nanoclusters. *Angew. Chem. , Int. Ed.* **2020**, *59*, 6507–6512.

[44] Cui, P.; Hu, H. S.; Zhao, B.; Miller, J. T.; Cheng, P.; Li, J. A multicentre-bonded [Zn^I]$_8$ cluster with cubic aromaticity. *Nat. Commun.* **2015**, *6*, 6331.

[45] Verma, G.; Forrest, K.; Carr, B. A.; Vardhan, H.; Ren, J. Y.; Pham, T.; Space, B.; Kumar, S.; Ma, S. Q. Indium-organic framework with *soc* topology as a versatile catalyst for highly efficient one-pot strecker synthesis of α-aminonitriles. *ACS Appl. Mater. Interfaces* **2021**, *13*, 52023–52033.

[46] Shi, W. Q.; Guan, Z. J.; Li, J. J.; Han, X. S.; Wang, Q. M. Site-specific doping of silver atoms into a Au_{25} nanocluster as directed by ligand binding preferences. *Chem. Sci.* **2022**, *13*, 5148–5154.

[47] AbdulHalim, L. G.; Ashraf, S.; Katsiev, K.; Kirmani, A. R.; Kothalawala, N.; Anjum, D. H.; Abbas, S.; Amassian, A.; Stellacci, F.; Dass, A. et al. A scalable synthesis of highly stable and water dispersible $Ag_{44}(SR)_{30}$ nanoclusters. *J. Mater. Chem. A* **2013**, *1*, 10148–10154.

[48] Yuan, S. F.; Lei, Z.; Guan, Z. J.; Wang, Q. M. Atomically precise preorganization of open metal sites on gold nanoclusters with high catalytic performance. *Angew. Chem. , Int. Ed.* **2021**, *60*, 5225–5229.

[49] Zhao, J. Q.; Han, M. F.; Zhao, X. J.; Ma, Y. Y.; Jing, C. Q.; Pan, H. M.; Li, D. Y.; Yue, C. Y.; Lei, X. W. Structural dimensionality modulation toward enhanced photoluminescence efficiencies of hybrid lead-free antimony halides. *Adv. Opt. Mater.* **2021**, *9*, 2100556.

[50] Xu, Y. X.; Chai, X. C.; Yang, W. T.; Hu, J. R.; Chen, J. N.; He, Y. B. Formation of a stable guanidinium-formamidinium phase in bismuth chloride perovskites with broadband emission. *Chem. Mater.* **2021**, *33*, 3258–3265.

[51] Wang, Z.; Li, X. Y.; Liu, L. W.; Yu, S. Q.; Feng, Z. Y.; Tung, C. H.; Sun, D. Beyond clusters: Supramolecular networks self-assembled from nanosized silver clusters and inorganic anions. *Chem.—Eur. J.* **2016**, *22*, 6830–6836.

[52] Li, X. Y.; Su, H. F.; Yu, K.; Tan, Y. Z.; Wang, X. P.; Zhao, Y. Q.; Sun, D.; Zheng, L. S. A platonic solid templating Archimedean solid: An unprecedented nanometre-sized Ag_{37} cluster. *Nanoscale* **2015**, *7*, 8284–8288.

Jin-Ping Gao received her M.S. degree from Shanxi Normal University in 2019. She will receive Ph.D. degree in inorganic chemistry from Shanxi Normal University under the guidance of Prof. Xian-Ming Zhang and Fu-Qiang Zhang in July 2023. Her research interest is syntheses and properties of Mo-POM templated high-nuclearity silver clusters.

Fu-Qiang Zhang received his M.S. degree from the department of chemistry of Inner Mongolia University in 2000 and Ph.D. degree in Shanxi Institute of Coal Chemistry, Chinese Academy of Sciences in 2006. He is a professor in the school of chemistry and material science as a faculty at Shanxi Normal University. His research focuses on DFT calculations of POMs and clusters.

Zhikai Qi received his M.S. degree in chemistry from Shanxi Normal University in 2014 and Ph.D. in materials science and engineering from University and Technology of China (USTC) in 2018. He then joined the school of chemistry and material science as a faculty at Shanxi Normal University. He is currently an associate professor and his research focuses on the low-dimensional hybrid metal halides and metal cluster-based luminescent materials.

Xian-Ming Zhang received his M.S. degree from Department of Chemistry, Inner Mongolia University in 1999 and Ph.D. degree in School of Chemistry and Chemical Engineering, Sun Yat-sen University under the guidance of Prof. Xiao-Ming Chen in 2002. He was awarded the "Humboldt" scholarship for postdoctoral research at the University of Heidelberg, Germany in April 2003 and was appointed as a professor in September 2003. His research interests include the metal–organic frameworks, covalent-organic frameworks, nonlinear optical crystals, and nanocluster chemistry. Prof. Zhang has published over 150 research papers, from 2014 to 2020, he has been listed in the "China's Highly Cited Scholars" list for seven consecutive years. He was awarded the second prize of the National Natural Science Award and the first prize and second prize of the Science and Technology Award of Shanxi Province.